Orbital Reconstruction and Interface Ferromagnetism in Self-Assembled Nanosheet Superlattices

Minoru Osada,[†,‡,*] Takayoshi Sasaki,[†,‡] Kanta Ono,[§] Yoshinori Kotani,[§] Shigenori Ueda,[⊥] and Keisuke Kobayashi[⊥]

[†]International Center for Materials Nanoarchitectonics (MANA), National Institute for Materials Science, Tsukuba, Ibaraki 305-0044, Japan, [‡]CREST, Japan Science and Technology Agency, Kawaguchi, Saitama 332-0012, Japan, [§]Institute of Materials Structure Science, High Energy Accelerator Research Organization, Tsukuba, Ibaraki 305-0801, Japan, and [⊥]NIMS Beamline Station at SPring-8, National Institute for Materials Science, Hyogo 679-5148, Japan

ABSTRACT We have investigated the interface electronic states in self-assembled $(Ti_{0.8}Co_{0.2}O_2/Ti_{0.6}Fe_{0.4}O_2)_n$ superlattices by X-ray photoelectron spectroscopy. A charge of about −0.3 electron is transferred from Fe to Co ions across the interface and induces a major reconstruction of the orbital occupation at the interfacial $(Ti_{0.8}Co_{0.2}O_2/Ti_{0.6}Fe_{0.4}O_2)$ layers. Supported by first-principles calculations, the Co^{3+} state is partially occupied at the interface by superlattice formation, and this new magnetic state directly influences the coupling between $Ti_{0.8}Co_{0.2}O_2$ and $Ti_{0.6}Fe_{0.4}O_2$ nanosheets. These data indicate that the orbital reconstruction is indeed realized by the interface charge transfer between Co and Fe ions in the adjoined nanosheets, and the generic feature of engineered interfaces can be extended to self-assembled superlattices of oxide nanosheets.

KEYWORDS: ferromagnetic nanosheets · layer-by-layer assembly · X-ray photoemission spectroscopy · orbital reconstruction · interface ferromagnetism

The synthesis of superlattices based on transition metal oxides has opened new pathways to interesting artificial materials with novel physical phenomena and new electronic states emerging at the interfaces.[1−8] Such oxide superlattices can provide a unique environment where the physical properties of interfaces may largely differ from and can even be orthogonal to those of bulk materials, due to the reconstruction of electronic states. The formation of high-mobility electron gas,[2,4] quantum Hall effect,[4,5] and even superconducting state[6] has been observed at the oxide interfaces. Underlying these studies is the technical prerequisite of the thin-film growth with single-unit-cell control and atomically sharp interfaces. This has been usually achieved by laser molecular-beam expitaxy,[9] which allows the tuning of physical properties while maintaining perfect crystal structure of the combined compounds.

Recent advances in two-dimensional (2D) oxide nanosheets offer an alternative opportunity for a similar layer-by-layer engineering.[10−15] Oxide nanosheets obtained *via* exfoliation of layered compounds possess a high 2D anisotropy with one-unit-cell thickness (typically ∼1 nm)[10] and, therefore, can be regarded as the thinnest self-standing 2D nanostructures having functionalities inherent from the parent compounds.[14,15] In addition, due to their polyelectrolytic nature, they can be employed as a building block for electrostatic layer-by-layer self-assembly.[12] Research in 2D nanosheets has recently intensified as a result of the successful exfoliation of functional oxides with various electronic properties including metallic,[16] semiconducting,[17] high-*k* dielectric,[18,19] redox-active,[20] and ferromagnetic.[21] These aspects make the nanosheet a suitable building block for designing superlattice films. Now, questions arise whether modification of electronic properties can be induced at such a self-assembled interface. This issue must be considered as an important factor in rational design of heterostructures with engineered physical properties using oxide nanosheets.

In this study, we present for the first time direct spectroscopic evidence for the interface electronic states in self-assembled superlattices of oxide nanosheets. The superlattice of ferromagnetic nanosheets ($Ti_{1-x}Co_xO_2$, $Ti_{1-x}Fe_xO_2$) is a model system to consider this issue because it exhibits a gigantic magneto-optical response (∼3 × 10^5 deg/cm) in the visible wavelength region, which stems from the interlayer $d-d$ transitions ($Co^{2+}-Fe^{3+}$) between adjacent nanosheets.[22] This superlattice is thus regarded as an artificially constructed ferromagnet, where the charge, spin, and orbital degrees of freedom might be strongly coupled at the interface. Here, we employed X-ray photoelectron analyses on self-assembled

* Address correspondence to osada.minoru@nims.go.jp.

Received for review March 2, 2011 and accepted August 8, 2011.

Published online August 08, 2011
10.1021/nn200835v

$(Ti_{0.8}Co_{0.2}O_2/Ti_{0.6}Fe_{0.4}O_2)_n$ superlattices and showed that the orbital reconstruction can be indeed realized by the interface charge transfer between Co and Fe ions in the adjoined nanosheets.

RESULTS AND DISCUSSION

Fabrication of Nanosheet Superlattice. A colloidal suspension of ferromagnetic nanosheets ($Ti_{0.8}Co_{0.2}O_2$, $Ti_{0.6}Fe_{0.4}O_2$) (Figure 1a) was prepared by delaminating layered titanates according to previously described procedures.[22] The superlattice films were fabricated *via* the sequential adsorption procedure reported previously.[12] Substrates such as atomically flat $SrTiO_3$ (Nb 0.5 wt %) ($SrTiO_3$:Nb) or quartz glass chips were primed with positively charged poly(diallyldimethylammonium) (PDDA). Ferromagnetic nanosheets were adsorbed in an alternate fashion from their colloidal suspension with intervention of dipping in a PDDA solution.

The superlattice assembly process of nanosheets was monitored by UV−visible absorption spectra. Figure 1b shows the buildup process of $(Ti_{0.8}Co_{0.2}O_2/Ti_{0.6}Fe_{0.4}O_2)_5$ superlattice on a quartz glass substrate. The spectral profile is similar for $Ti_{0.8}Co_{0.2}O_2$ and $Ti_{0.6}Fe_{0.4}O_2$, but a clear difference is observed at in-gap region (300−400 nm) due to the different $d-d$ transitions. In the $(Ti_{0.8}Co_{0.2}O_2/Ti_{0.6}Fe_{0.4}O_2)_5$ superlattice film, each deposition cycle causes progressive enhancements in absorbance for superlattice-type buildup, and the spectral profile observed can be understood in terms of the superimposition of the profile of each nanosheet.

The film quality of the superlattice films was characterized by atomic force microscopy (AFM), X-ray diffraction (XRD), and high-resolution transmission electron microscopy (HRTEM). An AFM image of nanosheets deposited on a $SrTiO_3$:Nb substrate clearly visualized the adsorbed nanosheets, which gave efficient surface coverage (>90%) of the substrate surface. XRD measurements detected a Bragg peak, which reflects a nanosheet/polycation nanostructure with the repeat distance of ~1.6 nm. Cross-sectional HRTEM observation provides direct information on the film structure. Figure 1c shows a HRTEM image of the $(Ti_{0.8}Co_{0.2}O_2/Ti_{0.6}Fe_{0.4}O_2)_5$ superlattice. The regular lamellar structure composed of nanosheets is clearly seen. The thicknesses of the constituent layers were approximately 1.6 nm, which are in good agreement with the interlayer distance (1.6 nm) in XRD diffraction data. We note that there are no detectable interdiffusion and strains at the interface, suggesting the production of a dead-layer-free superlattice directly assembled on the $SrTiO_3$:Nb substrate. Therefore, we may conclude that exact control of interface atomic stacking can be realized.

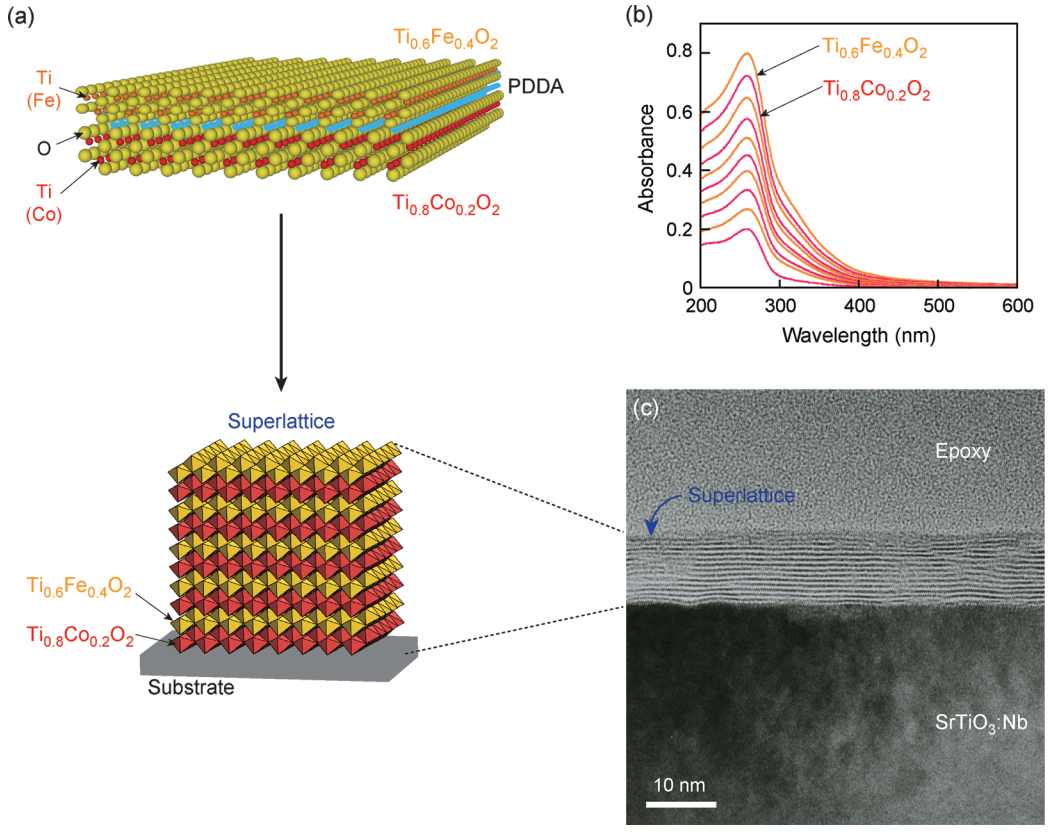

Figure 1. (a) Schematic view of the self-assembled superlattice of ferromagnetic nanosheets ($Ti_{0.8}Co_{0.2}O_2$, $Ti_{0.6}Fe_{0.4}O_2$). (b) Buildup process monitored with UV−visible spectroscopy in $(Ti_{0.8}Co_{0.2}O_2/Ti_{0.6}Fe_{0.4}O_2)_5$ superlattice on a quartz glass substrate. (c) HRTEM image of $(Ti_{0.8}Co_{0.2}O_2/Ti_{0.6}Fe_{0.4}O_2)$ superlattice on a $SrTiO_3$:Nb substrate.

A clear benefit of our approach is the experimental realization of the clean interface between superlattice and substrate. One of the most perplexing aspects of oxide thin films is the degradation of the interface. Current film-growth techniques require complex deposition processes with high-temperature post-annealing, producing large extrinsic effects arising from growth-induced defects and/or thermal strain. In that sense, our nanosheet superlattices are a unique system, in which soft-chemical layer-by-layer approach produces high-quality superlattices with an atomically sharp and clean interface. Such superlattices could eliminate the extrinsic origin arising from the substrates.

Magnetic properties were characterized by superconducting quantum interference device (SQUID) measurements. Superlattice $(Ti_{0.8}Co_{0.2}O_2/Ti_{0.6}Fe_{0.4}O_2)_n$ ($n = 5$) film exhibits room temperature ferromagnetism with the magnetic moment of $\sim$3.7 μ_B/Co,Fe, a value being surprisingly larger than those of multilayered films (1.4 μ_B/Co for $Ti_{0.8}Co_{0.2}O_2$, 0.7 μ_B/Fe for $Ti_{0.6}Fe_{0.4}O_2$).[22]

Spectroscopy at the Interface of the Nanosheet Superlattice. In order to discriminate the electronic structure at the interface from surface and bulk contributions, we have performed X-ray photoemission spectroscopy (PES) experiments (Figure 2) on $(Ti_{0.8}Co_{0.2}O_2/Ti_{0.6}Fe_{0.4}O_2)_n$ superlattices with different stacking sequences (n = 1, 5) by taking the advantage of the element specificity and varying probing depth of photoelectrons using hard X-ray PES (HX-PES) and soft X-ray PES (SX-PES). In particular, HX-PES is a new variant of the well-established photoemission technique, which extends its range to much higher photoelectron energies up to 10 keV and thus to enhanced probing depths of the order of 10 nm and beyond. This not only facilitates direct access to intrinsic electronic structures reflected on the entire volume of nanometer-thick films but also allows the study of buried interfaces not possible by conventional SX-PES.[23,24]

Figure 3a compares Co 2p core-level spectra of $(Ti_{0.8}Co_{0.2}O_2)_{10}$ multilayer film and $(Ti_{0.8}Co_{0.2}O_2/Ti_{0.6}Fe_{0.4}O_2)_5$ superlattice measured by HX-PES.

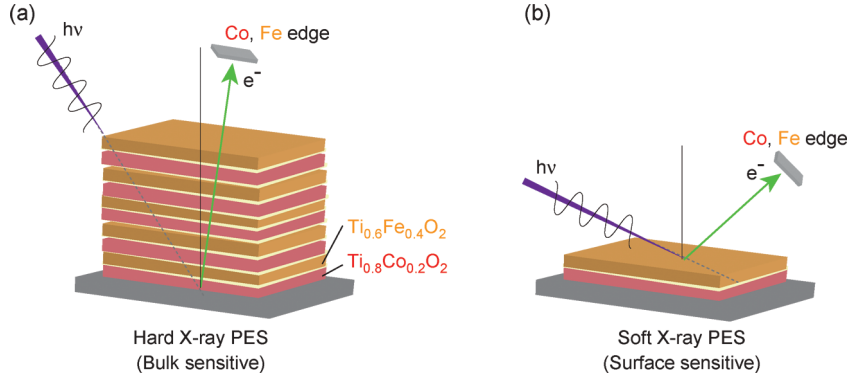

Figure 2. (a) Schematic of the experimental setup for characterization of interface electronic states in $(Ti_{0.8}Co_{0.2}O_2/Ti_{0.6}Fe_{0.4}O_2)_n$ superlattices (n = 5 and 1) using HX-PES (a) and SX-PES (b).

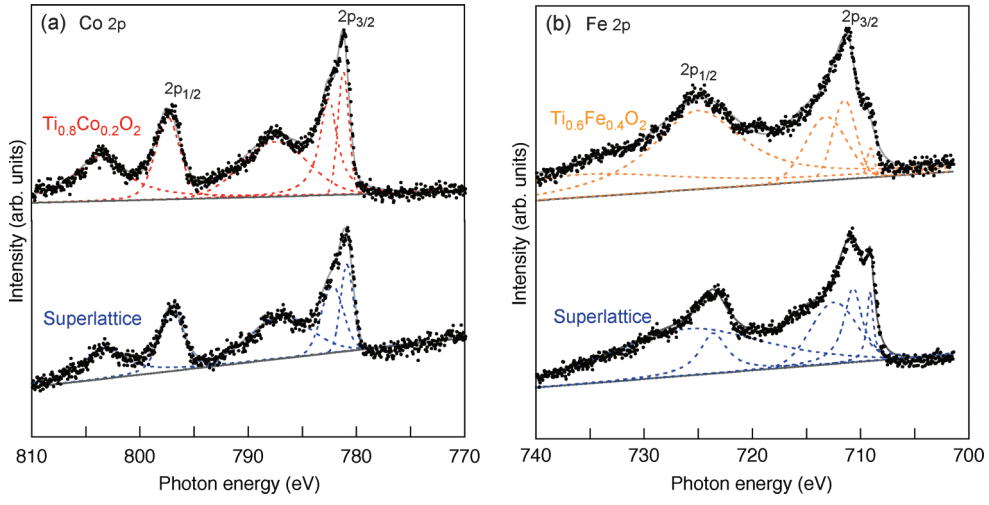

Figure 3. (a) HX-PES spectra at the Co 2p edge of the $(Ti_{0.8}Co_{0.2}O_2/Ti_{0.6}Fe_{0.4}O_2)_5$ superlattice and the $(Ti_{0.8}Co_{0.2}O_2)_{10}$ multilayer film. (b) HX-PES spectra at the Fe 2p edge of the $(Ti_{0.8}Co_{0.2}O_2/Ti_{0.6}Fe_{0.4}O_2)_5$ superlattice and the $(Ti_{0.6}Fe_{0.4}O_2)_{10}$ multilayer film. Fitting results are also included in each spectrum. We used a Gaussian convoluted with a Lorentzian to decompose multiplet structures.

We used a Gaussian convoluted with a Lorentzian to characterize multiplet structures and their peak energies. In $(Ti_{0.8}Co_{0.2}O_2)_{10}$ multilayer film, the Co 2p spectra show complex structures due to Coulomb interaction between Co 2p core hole and 3d electrons. Two peaks were observed in the XPS spectra at the binding energies of 797 and 781 eV corresponding to Co $2p_{1/2}$ and $2p_{3/2}$ core levels, respectively. In addition to the two spin−orbital components, two prominent satellite peaks were observed to be about 7 eV binding energy higher than both Co $2p_{1/2}$ and $2p_{3/2}$ main peaks. These satellite peaks reflect the different final states of Co due to a charge transfer between Co 3d and O 2p. From the comparison of spectral line shape and the peak position with those of other Co oxides containing different 3d counts (Figure S1 in Supporting Information), the spectrum shows a close resemblance to those of CoO and $CoTiO_3$ with Co^{2+}; the appearance of the satellite at ~787 eV is a signature for the Co^{2+} state. Thus, the oxidation state of doped Co ions in $Ti_{0.8}Co_{0.2}O_2$ nanosheets is found to be Co^{2+}, which is consistent with previous X-ray absorption experiments.[21,25]

The superlattice data are very different. We first notice that the Co $2p_{3/2}$ peak is shifted to lower energy with respect to the $(Ti_{0.8}Co_{0.2}O_2)_{10}$ multilayer film by 0.3 eV and that the high-energy shoulder reduces its intensity. A comparison to PES spectra of reference materials[26] containing Co^{2+} and Co^{3+} yields a rough estimate of $Co^{2.33+}$ (with an upper bound of $+0.33e$ per Co atom for the charge-transfer amplitude) (Figure S1b in Supporting Information). These results indicate that the charge is transferred across the interface and that a charged double layer is formed, as generally expected for heterostructures of materials with different work functions. Indeed, as a result of charge conservation, we observed the shift in Fe valence matching that of the Co ions in the $(Ti_{0.8}Co_{0.2}O_2/Ti_{0.6}Fe_{0.4}O_2)_n$ superlattice (Figure 3b). Because of the complex spectral feature and strong multiplet broadening of the Fe 2p peak, such a shift is much harder to recognize than in the case of Co, but the Fe $2p_{3/2}$ peak is clearly shifted to lower energy with respect to the $(Ti_{0.6}Fe_{0.4}O_2)_{10}$ multilayer film by 0.4 eV. From a comparison with reference spectra of materials containing Fe^{2+} and Fe^{3+} (Figure S2),[27] the low-energy shift in the Fe $2p_{3/2}$ peak is corresponding to a valence change from Fe^{3+} to Fe^{2+}. The shift of the Fe $2p_{3/2}$ edge of 0.5 eV translates into a lower bound of $-0.3e$ per Fe on the amplitude of the charge transfer across the interface, which is consistent with the estimated amplitude of $+0.33e$ based on the Co 2p spectra discussed above.

In order to obtain further information about the electronic states at the interface, we have carried out PES studies of bilayer $(Ti_{0.8}Co_{0.2}O_2/Ti_{0.6}Fe_{0.4}O_2)_1$ using SX-PES. We note that such a spectral change is not specific to the bulk-sensitive mode (HX-PES); a similar observation is also achieved in the surface-sensitive mode (SX-PES)[25] in bilayer $(Ti_{0.8}Co_{0.2}O_2/Ti_{0.6}Fe_{0.4}O_2)_1$ (Figure 4). The shifts of the Co and Fe core peaks are thus the evidence of a change in valence state of Co and Fe ions near the interface. Similar observations were also made on heterostructures by combining other ferromagnetic nanosheets ($Ti_{0.9}Co_{0.1}O_2$, $Ti_{0.8}Fe_{0.2}O_2$, $Ti_{0.7}Mn_{0.3}O_2$). The charge transfer is hence a general characteristic of ferromagnetic nanosheets.

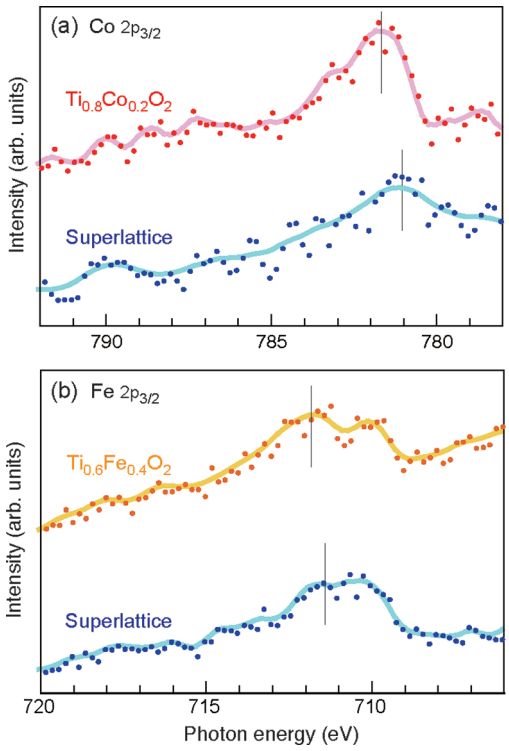

Figure 4. (a) SX-PES spectra at the Co 2p edge of the bilayer $(Ti_{0.8}Co_{0.2}O_2/Ti_{0.6}Fe_{0.4}O_2)_1$ and the monolayer $(Ti_{0.8}Co_{0.2}O_2)_1$. (b) SX-PES spectra at the Fe 2p edge of the bilayer $(Ti_{0.8}Co_{0.2}O_2/Ti_{0.6}Fe_{0.4}O_2)_1$ and the monolayer $(Ti_{0.6}Fe_{0.4}O_2)_1$. The shifts in the Co $2p_{3/2}$ and Fe $2p_{3/2}$ peaks observed in Figure 3 are also evident in the surface-sensitive mode (SX-PES) in the bilayer $(Ti_{0.8}Co_{0.2}O_2/Ti_{0.6}Fe_{0.4}O_2)_1$.

Further evidence for the interface charge transfer comes from valence-band spectra. Figure 5 shows valence-band spectra of the Co and Fe 3d band region. In $(Ti_{0.8}Co_{0.2}O_2)_{10}$ and $(Ti_{0.6}Fe_{0.4}O_2)_{10}$ multilayer films, there appears to be Co and Fe impurity bands at 3.68 and 2.04 eV, respectively. In the $(Ti_{0.8}Co_{0.2}O_2/Ti_{0.6}Fe_{0.4}O_2)_n$ superlattice, the valence spectrum shows Co and Fe impurity bands at 3.45 and 1.85 eV, both of which are shifted to lower energy with respect to the multilayer films by 0.2 eV. Such changes cannot be explained by a rigid-band model where the density of states is made up by superimposing those of $Ti_{0.8}Co_{0.2}O_2$ and $Ti_{0.6}Fe_{0.4}O_2$ nanosheets. A clear departure from the rigid-band model is another signature for the electronic reconstruction at the interface.

Interface Electronic States of Nanosheet Superlattice. Our data therefore imply that the electronic reconstruction

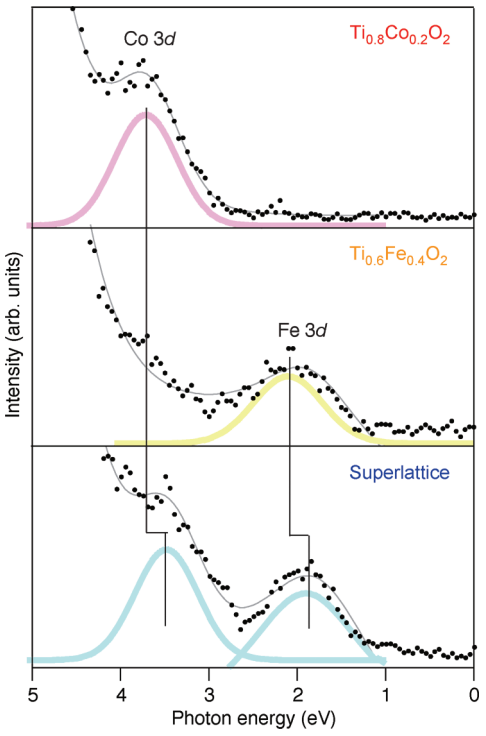

Figure 5. Valence-band spectra of (a) $(Ti_{0.8}Co_{0.2}O_2)_{10}$ multilayer film, (b) $(Ti_{0.6}Fe_{0.4}O_2)_{10}$ multilayer film, and (c) $(Ti_{0.8}Co_{0.2}O_2/Ti_{0.6}Fe_{0.4}O_2)_5$ superlattice.

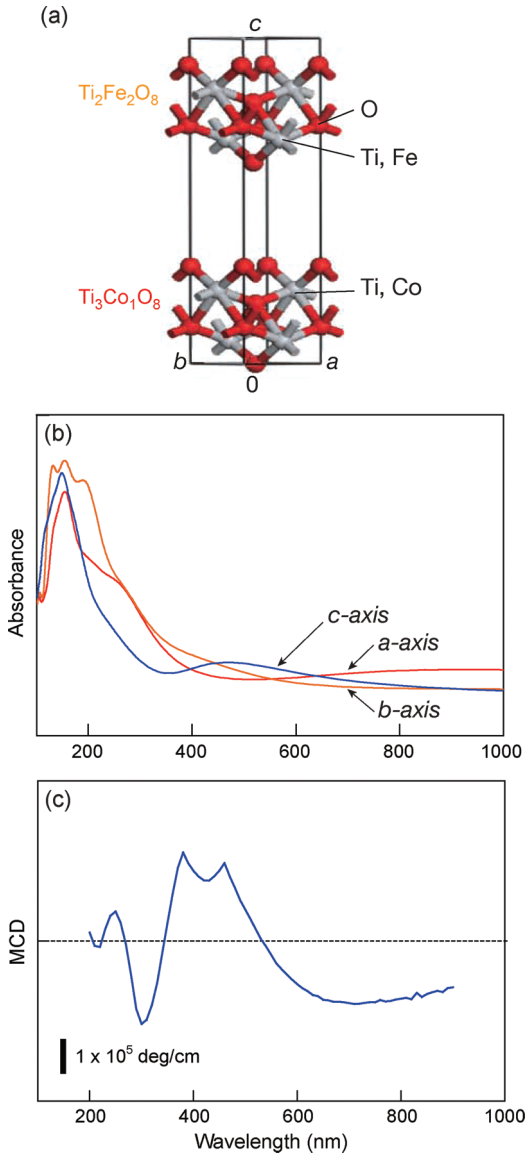

Figure 6. (a) Supercell used in the calculation for the $Ti_3Co_1O_8/Ti_2Fe_2O_8$ heterostructure. (b) Calculated optical absorption spectra of the $Ti_3Co_1O_8/Ti_2Fe_2O_8$ heterostructure. (c) Magnetic circular dichroism (MCD) spectrum of the $(Ti_{0.8}Co_{0.2}O_2/Ti_{0.6}Fe_{0.4}O_2)_5$ superlattice.

can be indeed realized by the interface charge transfer between Co and Fe ions in the adjoined nanosheets. The simplest view of our assembled superlattice is a stack of ferromagnetic nanosheets (1.1−1.2 nm) across intervening thin PDDA layers (0.4−0.5 nm), in which exchange interactions can be transmitted across the thin PDDA layers. To check whether the exchange-interaction scenario is viable, we performed a first-principle calculation[28,29] of the bilayer $Ti_3Co_1O_8/Ti_2Fe_2O_8$ ($Ti_{0.75}Co_{0.25}O_8/Ti_{0.5}Fe_{0.5}O_2$) (Figure 6). Bilayer $Ti_3Co_1O_8/Ti_2Fe_2O_8$ structure as shown in Figure 6a is modeled as a supercell. This calculation demonstrates that the formation of a strong hybridized bond between Co and Fe ions at the interface is indeed realistic (Figure 6b). Strong *d*−*d* absorption bands at 400−700 nm are a particular feature from the out-of-plane contribution (along *c*-axis) and attributed to the strongly hybridized band, indicating a strong spin−orbit interaction in the $(Ti,Co)O_2/(Ti,Fe)O_2$. We also note that the energies of the absorption components obtained by the first-principle calculation fairly agree with the observed features in magneto-optical spectra (Figure 6c). These facts suggest that the *d*−*d* transitions, despite their forbidden nature, can gain oscillator strength in intervalence charge transfers as the result of overlapping 3d orbitals. Such overlapping of 3d orbitals should enhance the exchange coupling between Co and Fe, which reconciling the observed enhancements of magneto-optical response in $(Ti_{0.8}Co_{0.2}O_2/Ti_{0.6}Fe_{0.4}O_2)_n$ superlattices.

To check this conjecture, we performed a model calculation of $Ti_{0.75}Co_{0.25}O_8$/(charged layer)/$Ti_{0.5}Fe_{0.5}O_2$ superlattices' intervening layers with thickness ranging from 0.1 to 1 nm. We investigated the dependence of separation distance on band structures. Figure 7a shows the variation of absorption spectra in $Ti_{0.75}Co_{0.25}O_8$/(charged layer)/$Ti_{0.5}Fe_{0.5}O_2$. We find that strong interactions occur for the distance of 0.2−0.7 nm where the strongly hybridized bands at 400−700 nm appeared in the out-of-plane component (along *c*-axis).[30] Figure 7b shows the dependence of the separation distance on absorption intensity and magnetic properties in the $Ti_{0.75}Co_{0.25}O_8$/(charged layer)/$Ti_{0.5}Fe_{0.5}O_2$. Clearly, the magnetic moment is greatly enhanced for the distance of 0.1−0.4 nm. The results indicate

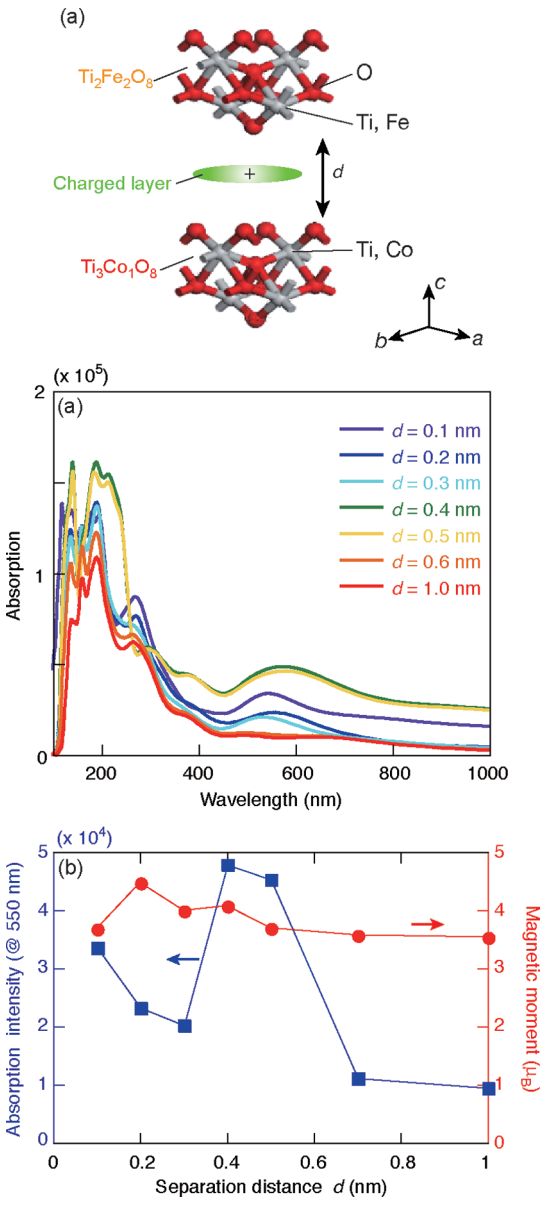

Figure 7. (a) Supercell used in the calculation for the $Ti_3Co_1O_8$/(charged layer)/$Ti_2Fe_2O_8$ heterostructure. (b) Calculated optical absorption spectra of the $Ti_3Co_1O_8$/(charged layer)/$Ti_2Fe_2O_8$ heterostructure with the separation distance ranging from 0.1 to 1 nm. (c) Comparison of absorption intensity at 550 nm and magnetic moment in the $Ti_3Co_1O_8$/(charged layer)/$Ti_2Fe_2O_8$.

that a strong hybridization between Co and Fe occurs for the distance of 0.2−0.4 nm, a value being close to the thickness of PDDA layers, and the exchange interaction can be transmitted across the very thin PDDA layers. In this case, the PDDA layers act as simple cations, which do not disturb the overlapping 3d orbitals.

In this context, we note that similar long-range exchange coupling exists in some metal complexes[31] and hybrid compounds;[32−34] interactions act over distances greater than 0.6 nm. In hybrid organic−inorganic layered ferromagnets with large interlayer spacing (>1 nm), it is shown that the exponential divergence of the in-plane

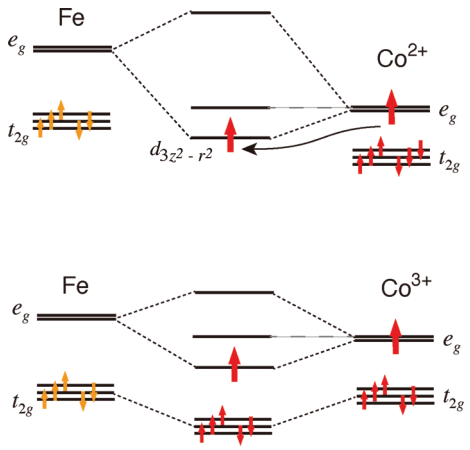

Figure 8. Schematic energy diagram showing the orbital reconstruction in the superlattice.

correlation length at low temperature promotes superspins within the magnetic layers which couple ferromagnetically through sizable dipolar interactions. This system also shows the occurrence of a spontaneous magnetization for a critical temperature that depends weakly on the distance between magnetic layers but mostly on the rate of divergence of the 2D correlation length, that is, on the strength of the in-plane exchange coupling. Due to the different materials with different spin states, the comparison should thus be viewed with some caution. However, the similarity in large interlayer spacing between our superlattice and these systems again points to the possible existence of long-range exchange interaction over PDDA layers.

We now focus on bringing these experimental and theoretical results together to help explain the orbital reconstruction in ($Ti_{0.8}Co_{0.2}O_2$/$Ti_{0.6}Fe_{0.4}O_2$) superlattices. Before the orbital reconstruction, the energy levels of t_{2g} and e_g orbitals in $Ti_{0.8}Co_{0.2}O_2$ are lower than those of $Ti_{0.6}Fe_{0.4}O_2$, as is also evident from valence-band spectra (Figure 5). In the ($Ti_{0.8}Co_{0.2}O_2$/$Ti_{0.6}Fe_{0.4}O_2$) heterointerface, the increase in Co oxidation state could raise the energy of the t_{2g} and e_g orbitals, which facilitates the hybridization between Co and Fe orbitals. We observed a clear signature for such an orbital reconstruction in valence-band spectra and calculated density of states (Figure S3 in Supporting Information). The prerequisite of the energy continuity at the interface suggests the possible energy alignment as shown in Figure 8, in which the strong hybridization between the Co and Fe orbitals forms the bonding $d_{3z^2-r^2}$ orbital (lower energy) and antibonding orbital (higher energy) at the interface. In the parent $(Ti_{0.8}Co_{0.2}O_2)_{10}$ and $(Ti_{0.6}Fe_{0.4}O_2)_{10}$ multilayer systems, the chemical states of doped Co and Fe ions are both in low-spin states with Co^{2+} ($t^6_{2g}e^1_g$, $S = 1/2$) and Fe^{3+} (t^5_{2g}, $S = 1/2$), respectively. Since molecular orbitals formed by e_g ($d_{3z^2-r^2}$) have the largest overlap at the interface, the bonding $d_{3z^2-r^2}$ orbital is occupied by an electron while the antibonding orbital is

unoccupied. The increase of Co valence results in the formation of the Co^{3+} state with a partially unoccupied t_{2g} orbital; the bonding $d_{3z^2-r^2}$ orbital is occupied by an electron whose spin is parallel to the localized t_{2g} spin in Co while the antibonding orbital is unoccupied. In the $Ti_{0.6}Fe_{0.4}O_2$ side with $(d_{3z^2-r^2})^0$, since there are unpaired electron t_{2g} orbitals, their spins align parallel to that of the electron in the bonding orbital due to the Hund coupling, This is equivalent to the Zener-type double-exchange interaction,[35] and the ferromagnetic coupling is generated in the ($Ti_{0.8}Co_{0.2}O_2$/$Ti_{0.6}Fe_{0.4}O_2$) heterointerface.

This type of the interface coupling seems to affect magnetic properties of the ($Ti_{0.8}Co_{0.2}O_2$/$Ti_{0.6}Fe_{0.4}O_2$) superlattice. Since our nanosheets are composed entirely of surface atoms arranged two-dimensionally, surface spins and their spin−orbit couplings are very strong. This situation is analogous to that in surface of $La_{1-x}Ca_xMnO_3$.[36] In such a case, the locally ferromagnetic coupling is very strong due to the unquenched orbital contributions, and the moment was enhanced by as much as 30% over the bulk value. In this context, the unoccupied t_{2g} orbitals in $Ti_{0.8}Co_{0.2}O_2$ nanosheets are expected to hybridize with the t_{2g} orbitals in $Ti_{0.6}Fe_{0.4}O_2$ and $Ti_{0.8}Co_{0.2}O_2$ nanosheets, permitting the $t_{2g}-t_{2g}$ hopping even inside nanosheets. In the ($Ti_{0.8}Co_{0.2}O_2$/$Ti_{0.6}Fe_{0.4}O_2$) superlattice, the induced magnetization is confined at the interface region, and the magnitude of the spin magnetization is likely to be enhanced.

This picture is in accordance with the dependence of oxidation states on magnetic properties of $Ti_{1-x}Co_xO_2$ and $Ti_{1-x}Fe_xO_2$ nanosheets with different oxidation states (Figure S4 in Supporting Information). We performed the first-principles calculation to investigate magnetic properties of $Ti_{1-x}Co_xO_2$ and $Ti_{1-x}Fe_xO_2$ nanosheets with different oxidation states. Our calculations indicate that the increase in the Co oxidation state greatly enhances the magnetization in the $Ti_{0.8}Co_{0.2}O_2$ nanosheet while the magnetization in the $Ti_{0.6}Fe_{0.4}O_2$ nanosheet is less sensitive to Fe oxidation state. This gives a qualitative picture why the interface charge transfer would enhance the magnetization in the $Ti_{0.8}Co_{0.2}O_2$/$Ti_{0.6}Fe_{0.4}O_2$ superlattice, which is consistent with microscopic SQUID and magneto-optical measurements. These results suggest that the orbital rearrangement and strong hybridization qualitatively explain the modification of the PES spectra at the interface and are responsible for the unusual magnetic behavior previously observed at the ($Ti_{0.8}Co_{0.2}O_2$/$Ti_{0.6}Fe_{0.4}O_2$) superlattices.

CONCLUSIONS

We have shown that the modification of electronic properties can be indeed realized at the self-assembled interface of oxide nanosheets. A charge of about $-0.3e$ is transferred from Fe to Co ions across the interface and induces a major reconstruction of the orbital occupation at the interfacial ($Ti_{0.8}Co_{0.2}O_2$/$Ti_{0.6}Fe_{0.4}O_2$) layers. We should emphasize that these interface features are not specific to material choice and interface geometry; similar interface reconstructions have been observed in the superlattices using other ferromagnetic nanosheets ($Ti_{0.9}Co_{0.1}O_2$, $Ti_{0.8}Fe_{0.2}O_2$, $Ti_{0.7}Mn_{0.3}O_2$). Also, the virtually infinite varieties of oxide nanosheets, which can be used to assemble interface, suggest that the charge-transfer interfaces will offer an unprecedented versatility for the realization of new 2D states. It seems definitely possible that high-mobility 2D electron gas and metallic conductivity will also occur at charge-transfer interfaces assembled from semiconducting and insulating oxide nanosheets.

METHODS

Synthesis of Ferromagnetic Nanohseets. Ferromagnetic nanosheets ($Ti_{0.8}Co_{0.2}O_2$, $Ti_{0.6}Fe_{0.4}O_2$) were synthesized by delaminating layered titanates according to previously described procedures.[22] The starting layered titanates ($K_{0.8}Ti_{1.6}Co_{0.4}O_4$, $K_{0.8}Ti_{1.2}Fe_{0.8}O_4$), prepared by a conventional solid state reaction, were converted into their protonic forms ($H_{0.8}Ti_{1.6}Co_{0.4}O_4 \cdot H_2O$, $H_{0.8}Ti_{1.2}Fe_{0.8}O_4 \cdot H_2O$) in HCl solution. Colloidal suspensions of $Ti_{0.8}Co_{0.2}O_2$ and $Ti_{0.6}Fe_{0.4}O_2$ nanosheets were synthesized by delaminating these protonic titanates with tetrabutylammonium hydroxide solution. Sectional analysis of atomic force microscopy revealed a sheet-like morphology (with the dimension of a few micrometers), which is inherited from the host layer in the parent compounds. The average thickness was 1.1 ± 0.1 nm for both cases. The values obtained are nearly comparable to the crystallographic thickness of the host layer in the corresponding parent compounds, supporting the formation of unilamellar nanosheets.

Fabrication of Superlattice Films. Superlattice films of $Ti_{0.8}Co_{0.2}O_2$ and $Ti_{0.6}Fe_{0.4}O_2$ nanosheets were fabricated by electrostatic layer-by-layer assembly technique previously described in detail.[12] An atomically flat $SrTiO_3$ (0.5% Nb-doped) ($SrTiO_3$:Nb) single crystal and a quartz glass chip were used as a substrate. Before the film deposition, the substrate (1 × 1 cm^2) was photochemically cleaned using ultraviolet light irradiation in ozone. The substrate was immersed in poly(diallyldimethylammonium) (PDDA) chloride solution (20 $g \cdot dm^{-3}$; pH = 9) for 20 min to attain a positively charged surface, followed by washing with copious amounts of pure water. Then, the substrate was dipped in a colloidal suspension of nanosheets (0.08 $g \cdot dm^{-3}$; pH = 9) for 20 min and washed again. The monolayer deposition for $Ti_{0.8}Co_{0.2}O_2$ and $Ti_{0.6}Fe_{0.4}O_2$ was repeated appropriate number of times (n) to produce a superlattice assembly composed of $(Ti_{0.8}Co_{0.2}O_2/Ti_{0.6}Fe_{0.4}O_2)_n$. For the use of references, multilayer films of $Ti_{0.8}Co_{0.2}O_2$ and $Ti_{0.6}Fe_{0.4}O_2$ nanosheets were also fabricated.

Characterization. The film quality of superlattice films was characterized by UV−visible spectroscopy, atomic force microscopy (AFM), X-ray diffraction (XRD), and high-resolution transmission electron microscopy (HRTEM). UV−visible absorption spectra were recorded in a transmission mode using a Hitachi U-4100 spectrophotometer. Film surface morphology was analyzed using an SII Nanotechnology E-sweep AFM. XRD patterns

were collected by a Rigaku RINT 2200 diffractometer using monochromatized Cu Kα radiation (λ = 0.15405 nm). Cross-sectional HRTEM was carried out using a Hitachi H-9000 microscope operating at 200 kV, which has a point resolution of 0.1 nm.

X-ray Photoemission Spectroscopy. Hard X-ray photoemission measurements were carried out at the undulator beamline BL15XU of SPring-8 Hyogo, Japan, at room temperature.[23,24] The excitation energy was set at 5956.4 eV, a choice yielding optimum energy resolution and that is well away from any absorption edge in $SrTiO_3$. The overall energy resolution was 230 meV. The photoemitted electrons were detected and analyzed for their kinetic energy by means of a hemispherical analyzer VG Scienta R4000. The angle between the incident X-rays and the direction of the detector was set at 88°. Binding energy was calibrated using the Fermi level of gold film. Complementary data were obtained by soft X-ray photoemission spectroscopy at SPring-8 BL17XU.

First-Principles Calculation. First-principles calculation was performed to investigate electronic structures in $Ti_{0.8}Co_{0.2}O_2$, $Ti_{0.6}Fe_{0.4}O_2$, and their heterostructures. We analyze the properties of these electronic structures related to ferromagnetism. The software package CASTEP[29] was used in our calculation. Bilayer $Ti_3Co_1O_8/Ti_2Fe_2O_8$ ($Ti_{0.74}Co_{0.25}O_2/Ti_{0.5}Fe_{0.5}O_2$) structure (as shown in Figure 6a) is modeled as a supercell. We also considered $Ti_3Co_1O_8$/(charged layer)/$Ti_2Fe_2O_8$ superlattices, in which charged layer slab with various thickness (0.1−1.0 nm) was inserted between $Ti_3Co_1O_8$ and $Ti_2Fe_2O_8$ layers. Valence states include 2s and 2p states for O (6 valence electrons) and 3s, 3p, 3d, and 4s states for Ti (12 valence electrons) and 3d and 4s for Fe and Co (8 and 9 valence electrons, respectively). The smooth parts of the wave functions were expanded in plane waves with a kinetic energy cutoff of 340 eV. The Brillouin zone sampling was performed by using a Monkhorst-Pack grid with a (4,5,1) grid of *k* points. The results are based on the fully optimized structure. The structural and ionic relaxations are alternatively performed on the supercell until the atomic forces are converged to 1×10^{-5} eV/atom. Spin-polarized calculations are also performed on the supercell. In order to simulate the models with real compositions ($Ti_{0.8}Co_{0.2}O_2$ and $Ti_{0.6}Fe_{0.4}O_2$), we also used the virtual crystal approximation (VCA) approach[30] established by Bellaiche and Vanderbilt for the study of properties of solid solutions in the context of density functional methods. We obtained almost identical results, indicating the validity for the $(Ti_3Co_1)O_8/(Ti_2Fe_2)O_8$ structure as a model supercell.

Complementary results were obtained from $Ti_{1-x}Co_xO_2$ and $Ti_{1-x}Fe_xO_2$ nanosheets with different oxidation states (Figure S3 in Supporting Information).

Acknowledgment. This work was supported by World Premier International Research Center Initiative (WPI Initiative in Materials Nanoarchitectonics), MEXT, CREST, JST, Grant-in-Aid for Scientific Research on Innovative Areas (Fusion Materials 2206) from MEXT, and the Industrial Technology Research Grant Program (06A22702d), NEDO, Japan. The XPS measurements were performed under the approval of NIMS Beamline Station (Proposal Nos. 2007A4608, 2007B4605, 2008A4602, and 2008A4800).

Supporting Information Available: Supplementary figures. This material is available free of charge *via* the Internet at http://pubs.acs.org.

REFERENCES AND NOTES

1. Heber, J. Materials Science: Enter the Oxides. *Nature* **2009**, *459*, 28–30.
2. Ohtomo, A.; Hwang, H. Y. A High-Mobility Electron Gas at the $LaAlO_3/SrTiO_3$ Heterointerface. *Nature* **2004**, *427*, 423–426.
3. Yamada, H.; Ogawa, Y.; Ishii, Y.; Sato, H.; Kawasaki, M.; Akoh, H.; Tokura, Y. Engineered Interface of Magnetic Oxides. *Science* **2004**, *305*, 646–648.
4. Tsukazaki, A.; Ohtomo, A.; Kita, T.; Ohno, Y.; Ohno, H.; Kawasaki, M. Quantum Hall Effect in Polar Oxide Heterostructures. *Science* **2007**, *315*, 1388–1391.
5. Tsukazaki, A.; Akasaka, S.; Nakahara, K.; Ohno, Y.; Ohno, H.; Maryenko, D.; Ohtomo, A.; Kawasaki, M. Observation of the Fractional Quantum Hall Effect in an Oxide. *Nat. Mater.* **2010**, *9*, 889–893.
6. Reyren, N.; Thiel, S.; Caviglia, A. D.; Kourkoutis, L. F.; Hammerl, G.; Richter, C.; Schneider, C. W.; Kopp, T.; Rüetschi, A. S.; Jaccard, D.; *et al.* Superconducting Interfaces between Insulating Oxides. *Science* **2007**, *317*, 1196–1199.
7. Brinkman, A.; Huijben, M.; van Zalk, M.; Huijben, J.; Zeitler, U.; Maan, J. C.; Van der Wiel, W. G.; Rijnders, G.; Blank, D. H. A.; Hilgenkamp, H. Magnetic Effects at the Interface between Non-magnetic Oxides. *Nat. Mater.* **2007**, *6*, 493–496.
8. Chakhalian, J.; Freeland, J. W.; Habermeier, H. U.; Cristiani, G.; Khaliullin, G.; van Veenendaal, M.; Keimer, B. Orbital Reconstruction and Covalent Bonding at an Oxide Interface. *Science* **2007**, *318*, 1114–1117.
9. Kawasaki, M.; Takahashi, K.; Maeda, T.; Tsuchiya, R.; Shinohara, M.; Ishiyama, O.; Yonezawa, T.; Yoshimoto, M.; Koinuma, H. Atomic Control of the $SrTiO_3$ Crystal Surface. *Science* **1994**, *266*, 1540–1542.
10. Sasaki, T.; Watanabe, M. Osmotic Swelling to Exfoliation. Exceptionally High Degrees of Hydration of a Layered Titanate. *J. Am. Chem. Soc.* **1998**, *120*, 4682–4689.
11. Schaak, R. E.; Mallouk, T. E. Perovskites by Design: A Toolbox of Solid-State Reactions. *Chem. Mater.* **2002**, *14*, 1455–1471.
12. Sasaki, T.; Ebina, Y.; Tanaka, T.; Harada, M.; Watanabe, M.; Decher, G. Layer-by-Layer Assembly of Titania Nanosheet/Polycation Composite Films. *Chem. Mater.* **2001**, *13*, 4661–4667.
13. Sasaki, T. Fabrication of Nanostructured Functional Materials Using Exfoliated Nanosheets as a Building Block. *J. Ceram. Soc. Jpn.* **2007**, *115*, 9–16.
14. Osada, M.; Sasaki, T. Exfoliated Oxide Nanosheets: New Solution to Nanoelectronics. *J. Mater. Chem.* **2009**, *19*, 2503–2511.
15. Ma, R.; Sasaki, T. Nanosheets of Oxides and Hydroxides: Ultimate 2D Charge-Bearing Functional Crystallites. *Adv. Mater.* **2010**, *22*, 5082–5104.
16. Sugimoto, W.; Iwata, H.; Yasunaga, Y.; Murakami, Y.; Takasu, Y. Preparation of Ruthenic Acid Nanosheets and Utilization of Its Interlayer Surface for Electrochemical Energy Storage. *Angew. Chem., Int. Ed.* **2003**, *42*, 4092–4096.
17. Sasaki, T.; Watanabe, M. Semiconductor Nanosheet Crystallites of Quasi-TiO_2 and Their Optical Properties. *J. Phys. Chem. B* **1997**, *101*, 10159–10161.
18. Osada, M.; Ebina, Y.; Funakubo, H.; Yokoyama, S.; Kiguchi, T.; Takada, K.; Sasaki, T. High-κ Dielectric Nanofilms Fabricated from Titania Nanosheets. *Adv. Mater.* **2006**, *18*, 1023–1027.
19. Osada, M.; Akatsuka, K.; Ebina, Y.; Funakubo, H.; Ono, K.; Takada, K.; Sasaki, T. Robust High-κ Response in Molecularly-Thin Perovskite Nanosheets. *ACS Nano* **2010**, *4*, 5225–5232.
20. Omomo, Y.; Sasaki, T.; Wang, L. Z.; Watanabe, M. Redoxable Nanosheet Crystallites of MnO_2 Derived *via* Delamination of a Layered Manganese Oxide. *J. Am. Chem. Soc.* **2003**, *125*, 3568–3575.
21. Osada, M.; Ebina, Y.; Fukuda, K.; Ono, K.; Takada, K.; Yamaura, K.; Takayama-Muromachi, E.; Sasaki, T. Ferromagnetism in Two-Dimensional $Ti_{0.8}Co_{0.2}O_2$ Nanosheets. *Phys. Rev. B* **2006**, *73*, 153301-1−4.
22. Osada, M.; Ebina, Y.; Takada, K.; Sasaki, T. Gigantic Magneto-Optical Effects in Multilayer Assemblies of Two-Dimensional Titania Nanosheets. *Adv. Mater.* **2006**, *18*, 295–299.
23. Kobayashi, K.; Yabashi, M.; Takata, Y.; Tokushima, T.; Shin, S.; Tamasaku, K.; Miwa, D.; Ishikawa, T.; Nohira, H.; Hattori, T.; *et al.* High Resolution-High Energy X-ray Photoelectron Spectroscopy Using Third-Generation Synchrotron Radiation Source, and Its Application to Si-High k Insulator Systems. *Appl. Phys. Lett.* **2003**, *83*, 1005–1007.
24. Takata, Y.; Tamasaku, K.; Tokushima, T.; Miwa, D.; Shin, S.; Ishikawa, T.; Yabashi, M.; Kobayashi, K.; Kim, J. J.; Yao, T.;

et al. A Probe of Intrinsic Valence Band Electronic Structure: Hard X-ray Photoemission. *Appl. Phys. Lett.* **2004**, *84*, 4310–4312.
25. Kotani, Y.; Taniuchi, T.; Osada, M.; Sasaki, T.; Kotsugi, M.; Guo, F. Z.; Watanabe, Y.; Kubota, M.; Ono, K. X-ray Nanospectroscopic Characterization of a Molecularly Thin Ferromagnetic $Ti_{1-x}Co_xO_2$ Nanosheet. *Appl. Phys. Lett.* **2008**, *93*, 093112.
26. McIntyre, N. S.; Cook., M. G. X-ray Photoelectron Studies on Some Oxides and Hydroxides of Cobalt, Nickel, and Copper. *Anal. Chem.* **1975**, *47*, 2208–2213.
27. McIntyre, N. S.; Zetaruk, D. G. X-ray Photoelectron Spectroscopic Studies of Iron Oxides. *Anal. Chem.* **1977**, *49*, 1521–1529.
28. Sato, H.; Ono, K.; Sasaki, T.; Yamagishi, A. First-Principles Study of Two-Dimensional Titanium Dioxides. *J. Phys. Chem. B* **2003**, *107*, 9824–9828.
29. Bellaiche, L.; Vanderbilt, D. Virtual Crystal Approximation Revisited: Application to Dielectric and Piezoelectric Properties of Perovskites. *Phys. Rev. B* **2000**, *61*, 7877–7882.
30. We have also checked another model where Co ions are assigned to the far sides from the interface. We find that strong interactions occur for the distance of 0−0.5 nm, a value being close to the thickness of PDDA layers.
31. Coffman, R. E.; Buettnerz, G. R. A Limit Function for Long-Range Ferromagnetic and Antiferromagnetic Superexchange. *J. Phys. Chem.* **1979**, *18*, 2387–2392.
32. Drillon, M.; Panissod, P. Long-Range Ferromagnetism in Hybrid Compounds: The Role of Dipolar Interactions. *J. Magn. Magn. Mater.* **1998**, *188*, 93–99.
33. Fujita, W.; Awaga, K. Magnetic Properties of $Cu_2(OH)_3$-(Alkanecarboxylate) Compounds: Drastic Modifications with Extension of the Alkyl Chain. *Inorg. Chem.* **1996**, *35*, 1915–1917.
34. Laget, V.; Hornick, C.; Rabu, P.; Drillon, M. Hybrid Organic−Inorganic Layered Coumpounds Prepared by Anion Exchange Reaction: Correlation between Structure and Magnetic Properties. *J. Mater. Chem.* **1999**, *9*, 169–174.
35. Zener, C. Interaction between the d-Shells in the Transition Metals. II. Ferromagnetic Compounds of Manganese with Perovskite Structure. *Phys. Rev.* **1951**, *82*, 403–405.
36. Filippetti, A.; Pickett, W. E. Double Exchange Driven Spin Pairing at the (001) Surface of Manganites. *Phys. Rev. B* **2000**, *62*, 11571–11575.